Influence of Al$_2$O$_3$ Particle Size on Microstructure, Mechanical Properties and Abrasive Wear Behavior of Flame-Sprayed and Remelted NiCrBSi Coatings

K.A. Habib, D.L. Cano, C.T. Caudet, M.S. Damra, I. Cervera, J. Bellés, and P. Ortells

The influence of micrometric alumina (low surface area-to-volume ratio) and nanometric alumina (high surface area-to-volume ratio) on microstructure, hardness and abrasive wear of a NiCrBSi hardfacing alloy coating applied to an AISI 304 substrate using flame spraying (FS) combined with surface flame melting (SFM) is studied. Remelting after spraying improved the mechanical and tribological properties of the coatings. Microstructural characterization using XRD, SEM and EDS indicated that alumina additions produced similar phases (NiSi, Ni$_3$B, CrC and Ni$_{31}$Si$_{12}$) regardless of the alumina size, but the phases differed in morphology, size distribution and relative proportions from one coating to another. The addition of 12 wt.% nanometric Al$_2$O$_3$ increased the phases concentration more than five- to sixfold and reduced the hard phases size about four-to threefold compared with NiCrBSi + 12 wt.% micrometric Al$_2$O$_3$. Nanoalumina led to reduced mass loss during abrasive wear compared to micrometric alumina and greater improvement in hardness.

1. Introduction

Wear-resistant hard coatings obtained by different reinforcement powders are applicable in many fields of industry. NiCrBSi coatings are widely used to improve the quality of components whose surface is subjected to severe work conditions such as coal-fired boilers, heat exchangers, turbines, tools, extruders, plungers, roller tables, piston rings, wearing plates, pump shafts, agriculture machinery (Ref [1], [2]). Nickel-based alloys used either on their own or combined with other reinforcement particles have become popular because of both outstanding wear and corrosion resistance at high temperatures and relatively low cost (Ref [3-6]). Such protective coatings are applied for original part production as well as for restoration purposes.

In recent years, the use of thermal spraying techniques for the application of self-fluxing (SFA) NiCrBSi coatings has increased enormously (Ref [7-10]). Nevertheless, some results show that, despite the introduction of new deposition methods such as high-velocity oxy-fuel, thermal-sprayed Ni-based coatings have low to moderate adhesion to the substrate, porosity and form oxide interlayers (Ref [11-14]), which impair their properties. As a result, subsequent melting could be necessary to reduce the porosity and improve their tribological properties. There are a considerable number of techniques to melt and propel the coating material. Flame spray is the one most commonly applied (Ref [15]). It is also one of the most economical and can be applied to a wide range of materials.

Many researchers have studied the addition of different types of reinforcement in order to improve the wear resistance of SFA coatings (Ref [16-18]). Carbides (Ref [16-19]) and carbide-based cermets, mostly WC-Co (Ref [19-22]), are used as hard particles in the majority of cases. However, the usage of WC or WC-Co entails some problems, such as loss of carbon and formation of brittle W$_2$C phase (Ref [16]). This is why studying the alternatives, such as TiC- and Cr$_2$C$_3$-based materials (Ref [23]) was considered important. Previously, the addition of TiC-NiMo and Cr$_2$C$_3$-Ni cermet particles proved to enhance the abrasive wear resistance of Ni-based SFA HVOF coatings up to 2 times (Ref [24]). Anyway, a central problem with the carbide reinforcement is the dissolution of the carbide particles (Ref [25]) that results in lowered wear resistance, as there are less remaining metallic carbides to reinforce the material to protect the coatings (Ref [26]). Carbide particle dissolution occurs when enough heat is attained, above a critical temperature (Ref [27]). In order to avoid this problem, oxide ceramics such as alumina, zirconia, titania, chromia, silica and yttria have been also widely used as coating materials to improve wear, erosion, cavitation, fretting and corrosion resistance (Ref [28-30]). Other researchers have studied the particle volume fraction, size and stiffness on wear resistance of particle-reinforced composites (Ref [31]). Natarajan et al. investigated the effect of graphite addition on the microstructure, hardness and abrasive wear behavior of flame-sprayed NiCrBSi coatings (Ref [32]). Harsha et al. also studied the influence of the WC particle addition on the microstructure, microhardness and abrasive wear behavior of flame-sprayed Co-Cr-W-Ni-C (EWAC 1006) coatings deposited on low-carbon steel substrate (Ref [33]). A review of technical literature regarding cermet coatings after it is sprayed and remelted does not address the question concerning the influence of reinforcement particles surface area on the microstructure and abrasive wear behavior of these coatings.

K.A. Habib, D.L. Cano, C.T. Caudet, M.S. Damra, I. Cervera, J. Bellés, and **P. Ortells,** Department of Industrial System Engineering and Design, Universitat Jaume I, 12071 Castellón, Spain. Contact e-mail: razzaq@esid.uji.es.

In the current work, a comparison of the abrasive wear behavior of NiCrBSi coatings deposited by flame spray technique and reinforced with micro- and nanometric particles of alumina is made with the aim of establishing the relationship between the tribological response of the material and the influence of Al_2O_3 particles surface area.
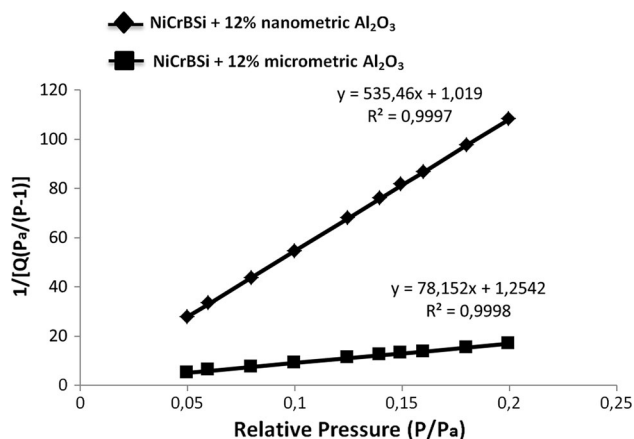
2. The Experimental Procedure

2.1 Materials

A NiCrBSi Castolin PE 3307 alloy with an average grain size range of 125/45 μm and melting point of 1025º C was used as metal matrix, and its nominal chemical composition in weight is: 0.4% C, 3.1% Si, 1.6% B, 10.1% Cr, 2.8% Fe and Ni rest. Spherical micro-Al_2O_3 (PRAXAIR ALO-101, ALO-325 mesh) and nano-Al_2O_3 (NANOX S2600S) were used as reinforcement ceramic phase, in order to obtain two different coatings (NiCrBSi + micrometric Al_2O_3 and NiCrBSi + nanometric Al_2O_3).

Powder mixture of commercial NiCrBSi alloy (88 wt.%) and micro- and nanometric Al_2O_3 (12 wt.%) was prepared with a Turbula rotative mixer, for 4 h at 300 rpm, in order to obtain an homogeneous powder.

2.2 Al_2O_3 Surface Area Determination

In order to compare the surface area of micro- and nanometric Al_2O_3-strengthened NiCrBSi spray powder, N_2 adsorption measurements were taken at 77 K using an Accelerated Surface Area and Porosimetry Analyzer (ASAP 2020; Micrometritics Instrument Corp.). The N_2 adsorption technique quantifies the surface area and porosity characteristics by measuring the amount of N_2 adsorbed and desorbed onto a porous solid material over a wide range of relative pressures P/P_o from 10 to 1 (where P is the equilibrium pressure and P_o is the saturation pressure). The adsorption isotherms obtained from these measurements allow to determine the surface area, pore volume, and pore size distributions (PSDs) (Ref 34-36). The specific surface area is calculated based on Brunauer, Emmett and Teller (BET) theory (Ref 37) from the linear part of the adsorption isotherm, at pressures $0.05 < P/P_o < 0.30$. According to Fig. 1, nanometric Al_2O_3 has a greater surface area compared to the micrometric Al_2O_3.

2.3 Thermal Spray

AISI 304 test specimens of 8 mm diameter and 18 mm length were grit-blasted with corundum particles of 99.6% purity and mean size of 0.53 mm, using 0.4 MPa air pressure, incidence angle of ∼ 45° and gun-to-substrate distance of 130 mm. The surface was then cleaned and degreased using acetone within an ultrasonic bath. The average surface roughness was 5.1 ± 0.5 μm, and the mean roughness depth (defined as the vertical distance between the highest peak and deepest valley) was 28.3 ± 2.4 μm. They were measured using a profilometer (Perthometer M1, Mahr GMBH, Germany).

Coatings were all deposited with a CDS-8000 flame spray gun, made by Castolin Eutectic. Thermal spray parameters are shown in Table 1. After the flame spraying process (FS), coatings underwent surface flame melting (SFM). Furthermore, other samples were coated with commercial NiCrBSi (unmodified) powders to evaluate the effect of dispersed micro- and nanometric Al_2O_3 reinforcement on abrasive wear behavior.

The melting process was performed using the surface flame melting (SFM) with scanning speed of approximately 150 mm/min. The coatings obtained were about 1.5 mm thick.

2.4 Methodology of XRD Measurement

The crystalline phases of the initial sprayed powder and after remelting were analyzed by x-ray diffraction (XRD), using a D5000D diffractometer by Siemens (Germany), employed at ambient temperature with an intensity scanner vs. diffraction angle between 5° and 70° (step size of 0.050°, scanner velocity = 3 s/step) using copper Kα radiation (λ = 1.5406 Å), a voltage of 40 kV and a 30 mA filament current.

2.5 Microhardness

Vickers microhardness testing was conducted using a Shimadzu tester applying 200 g load during 15 s to determine the microhardness profile along the cross section of deposited coatings from the substrate base metal to the coatings surface. At least six measurements were taken in each distance, and the average values have been taken in this study.

2.6 Abrasive Wear Test

Abrasive wear tests were conducted on a TE79/P pin-on-disk multi-axis tribometer from Plint and Parteners under room temperature and humidity. Self-fluxing NiCrBSi alloy 12%

Fig. 1 BET plot of N_2 adsorption and desorption isotherms of nanometric and micrometric Al_2O_3 dispersion-strengthened NiCrBSi spray powder

Table 1 Thermal spray parameters

Gun speed, mm/s	Number of strokes	Distance, mm	Acetylene pressure, bar	Oxygen pressure, bar	Air pressure, bar	Flame type
67.5	5	120	0.7	4	2.5	Neutral

dispersed alumina (micro- and nanoparticles), over stainless steel pins were slid under a 5, 10 and 20 N load against a SiC disk (Buehler metallographic abrasive, 400 GRIT 100 μm). A new abrasive disk was used for each 10-m test run, in order to provide fresh abrasives over a sliding distance of 100 m. The loss of material was determined by weighting the samples before and after the tests, and ultrasonic cleaning was carried out for each of them. Three abrasion tests were performed for each type of samples, and their results were reproducible within 5% deviation. The width of the wear track was also measured at the end of each test so as to calculate the total volume worn away in line with the recommendation of the ASTM G77 norms.

3. Results and Discussion

3.1 Microstructural Characterization

3.1.1 XRD Analysis. The comparison of x-ray diffraction patterns for each coating and the initial powder are shown in Fig. 2. It can be observed that Ni and Cr peaks are detected in the x-ray diffraction analysis of the initial powder and the same peaks, even weaker, are observed in the deposits. With reference to the original powder, the results show that the biggest peaks correspond to Ni and also to the Cr solid solution in Ni matrix. On the other hand, two Cr peaks exist, which can be attributed to BCr and SiCr.
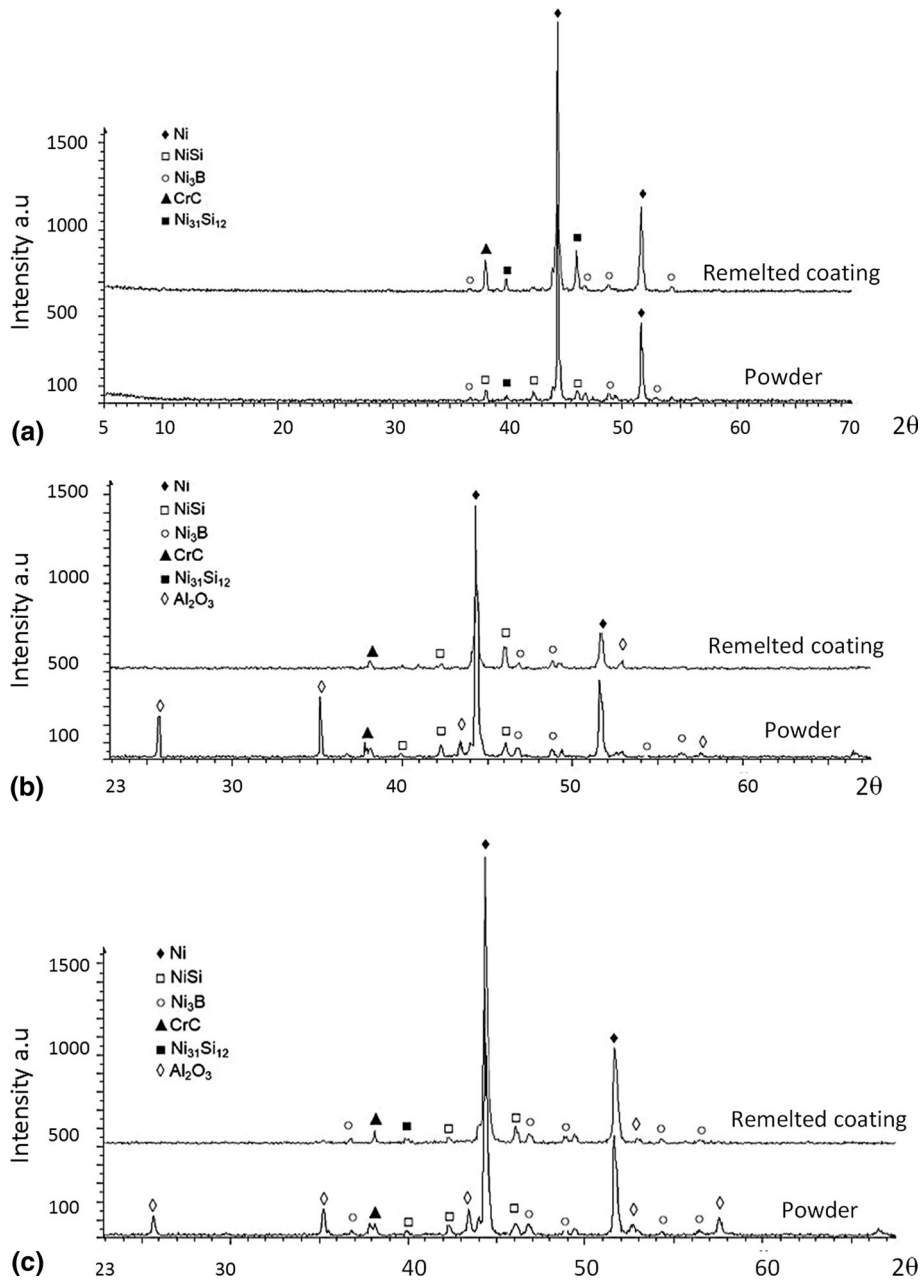
Fig. 2 X-ray diffraction for the NiCrBSi-Al$_2$O$_3$ coatings on AISI 304: (a) no modified NiCrBSi, (b) NiCrBSi + 12% micrometric Al$_2$O$_3$ and (c) NiCrBSi + 12% nanometric Al$_2$O$_3$

In Fig. 2(a), two spectra of commercial powder and NiCrBSi coating can be seen. The one at the bottom shows the powder diffraction peaks and the top one shows XRD spectra of remelted coating. As it can be expected in all three cases, Fig. 2(a), (b) and (c), Ni peaks are the strongest. We can see a small Cr peak at 49° and at about 45° chromium peak overlaps with the strong Ni peak. There are some minor peaks in all three spectra. These belong to borides, carbides and silicates. It can be observed that no significant changes occur in diffractograms after the remelting process of NiCrBSi coating. Ni peaks are still the most intense, and there is just small increase in their width. It can indicate slight amorphization during deposition and remelting processes. Smaller peaks of CrC, Ni_3B and NiSi can hardly be detected in the diffractograms of the remelted coating. It is possible that decomposition of some of those compounds had taken place during the coat deposition and remelting processes.

In Fig. 2(b) and (c), the addition of 12% of micrometric (lower-alumina surface area) and nanometric (higher-alumina surface area) results in appearance of alumina peaks. In remelted coating diffractograms, these peaks are relatively weak. It can be explained by the gradual separation of NiCrBSi and Al_2O_3 during deposition and remelting processes, because of the different particle size and different mass of the powders mixed. Smaller peaks of CrC, Ni_3B and NiSi appear in all of diffractograms, and no major changes occur.

Generally speaking, the solid solution is created during the cooling period of the atomization process. The slow cooling rate allows the precipitation of Ni_xB and NiSi phases because of their low melting point (Ref 38, 39). That is, during the spray, the powder is completely melted inducing the dissolution of borides and silicides in the liquid phase. It must be underlined that the presence of B and Si elements makes difficult the crystallization phenomena. With reference to previous works (Ref 40, 41), when the cooling rate increases, a crystallization process becomes impossible and amorphous formation conditions are satisfied. Then, during the cooling of the particles just after impacting the substrate, this building material presents an amorphous structure if its cooling rate is relatively high. The cooling rate is also influenced by the thickness of the splats. When a critical thickness is reached, the contact surface between the particle and the substrate is reduced, leading to a lower cooling rate and thus the crystallization process occurs.

3.1.2 Coatings Microstructure. The general view of the coatings cross section is shown in Fig. 3. The porosity of remelted coatings is generally low and can be observed in the upper part of the deposited coating, but the overall homogeneity is quite good, as the splat boundaries disappeared in consequence of fusing process. Moreover, the absence of cracking or delamination and the good bond with the substrate show that the processing parameters selected in this study have ensured high-quality coatings. The boundary roughness between coating and substrate is preserved; no metallurgical bonding can be expected due to flame remelting process.

The SEM image of unmodified NiCrBSi coating, Fig. 4, shows a homogenous microstructure and some porosity. As seen in the EDX, this microstructure based on Ni matrix is rich in Cr and poor in Fe and Si. The randomly scattered and relatively darker gray phase contains Ni, Cr, C, Si and Fe as well as other compounds based on chromium carbides and borides or even amorphous phases along the grain boundaries. EDS spot analysis were performed to identify the chemical composition of different phases, and the corresponding results are listed in Table 2.

In Fig. 5, corresponding to the NiCrBSi + 12% micrometric Al_2O_3 coatings the melted zone has a homogenous distribution of Cr precipitation of blocky morphology (light gray). X-ray point microanalysis and chemical mapping of this zone indicate that the Cr solid solution contains Ni (28.36 wt.%), C (15.31 wt.%), Si (2.29 wt.%) and Fe (2.29 wt.%). The micrometric alumina is black-colored and randomly scattered.
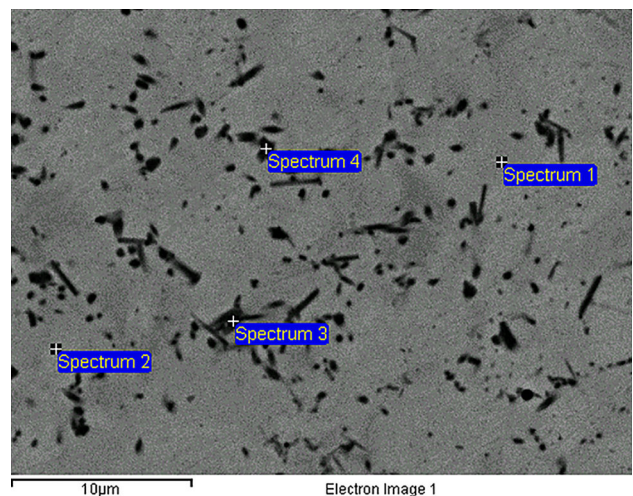

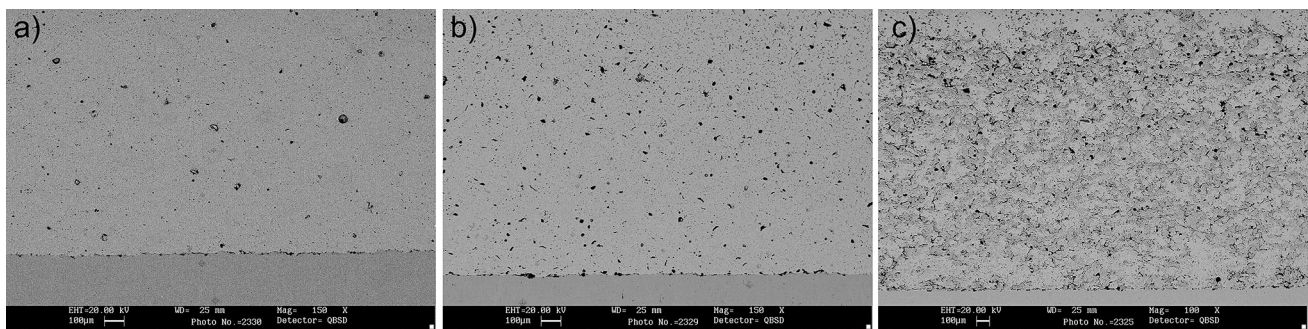**Fig. 4** SEM micrograph of melted NiCrBSi coating

Fig. 3 SEM images showing morphologies of: (a) unmodified NiCrBSi, (b) NiCrBSi + 12% micrometric alumina and (c) NiCrBSi + 12% nanometric alumina

Table 2 Chemical composition (wt.%) of remelted NiCrBSi coating

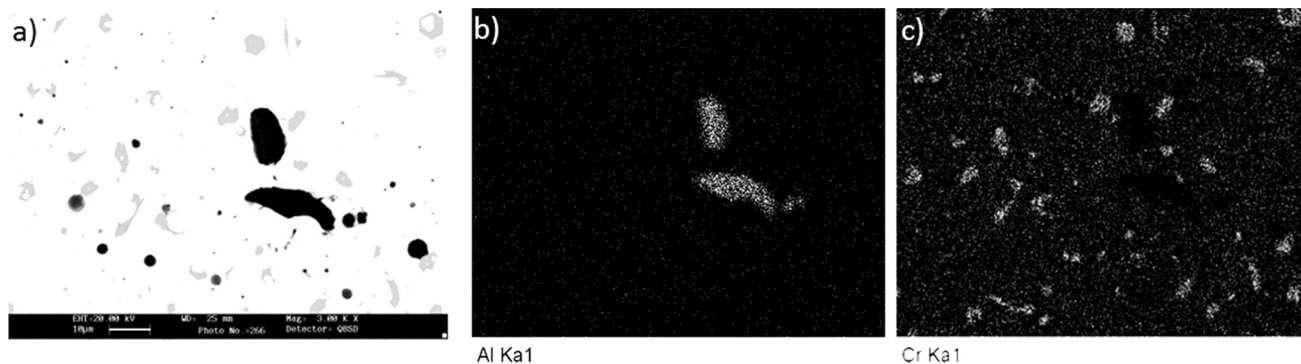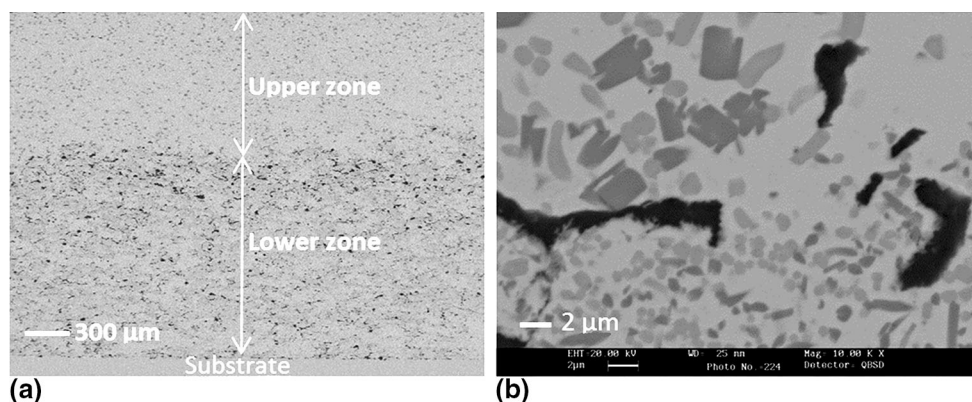| Elements	C	O	Si	Cr	Fe	Ni
Spectrum 1	11.14	2.80	1.53	37.87	2.08	44.58
Spectrum 2	8.31		2.20	22.04	2.87	64.58
Spectrum 3	7.89		3.01	7.69	2.48	78.94
Spectrum 4	12.74		1.97	20.49	1.95	62.84

Fig. 5 Mapping of Al and Cr elements distribution of NiCrBSi + 12% micrometric Al_2O_3

Fig. 6 MEB image of microstructure of upper and lower parts of NiCrBSi + 12% nanometric Al_2O_3 coating

Figure 6 shows the microstructure of the NiCrBSi + 12% nanometric Al_2O_3 coating. The remelting zone has a non-homogenous microstructure, probably because of the local change in solidification conditions (Ref 42, 43). It can be observed that the lower zone is around 0.9 mm thick and their microstructural constituents are a homogenous distribution of small precipitation (1-2 μm) on Cr and Ni metal matrix, Fig. 6 and 7. The thin Cr precipitation has been formed at the substrate interface (lower zone) because of the metal carbides formation during the melting process and higher surface area of well-distributed nanometric alumina (Fig. 8). This fact accelerates the nucleation and acts as a heat sink (high undercooling), where the temperature gradient (G) is fairly low and the solidification velocity (v) is relatively high, with a sufficient low G/v ratio. Figure 7 shows the chemical mapping of Al and Cr elements distribution of NiCrBSi + 12% nanometric Al_2O_3.

X-ray point microanalysis, Fig. 9(a), reveals that the microstructure of the NiCrBSi + 12% nanometric alumina consists mainly of a Ni-based matrix with Cr (7.86 wt.%), Fe (5.06 wt.%) and Si (3.65 wt.%). Coarse dark gray phase (1) contains Cr (67.98 wt.%), Ni (29.23 wt.%), B (1.88 wt.%) and Si (0.9 wt.%); light gray phase (2) principally consists of Cr (68.15 wt.%), C (17.21 wt.%), Ni (11.75 wt.%) and Fe (2.89 wt.%); and finally black phase (3) consists of alumina. Immediately above this layer (upper zone), higher inhomogeneity is shown. This is mostly due to the increasing size of hard inclusions (5-6 μm) and their different shapes. The microstructural changes usually are related to the change in the solidification condition, which means that the temperature gradient (G) is fairly high and the solidification velocity (v) is relatively low (low undercooling).

So the reinforcement particles below a certain size (with enough surface area) are pushed of solidification front and can act to restrict the precipitates grain growth. At the same point, the energy required to push the particles will be less than that for dendrite, to branch out from same gap in the surrounding particles and nucleate a new grain. This mechanism results in a smaller grain size and thus increased strength. If one could get
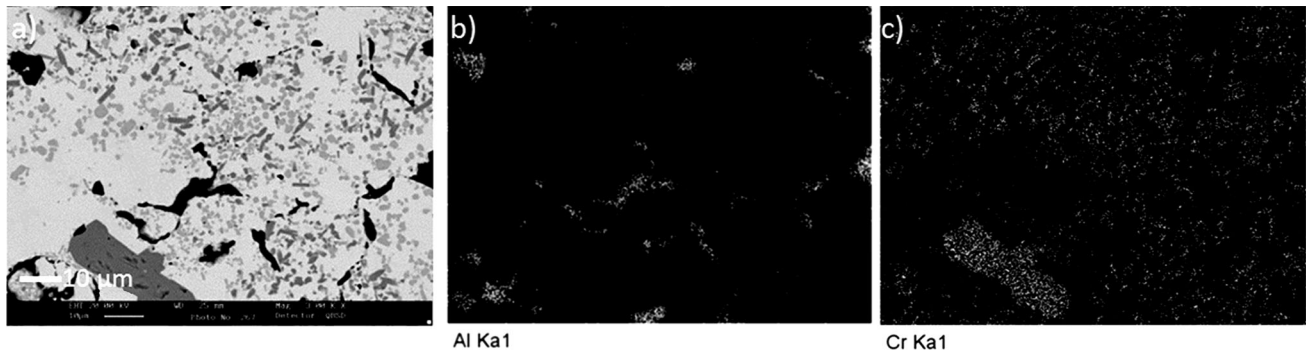
Fig. 7 Chemical mapping of Al and Cr elements distribution of NiCrBSi + 12% nanometric Al_2O_3 (lower zone)
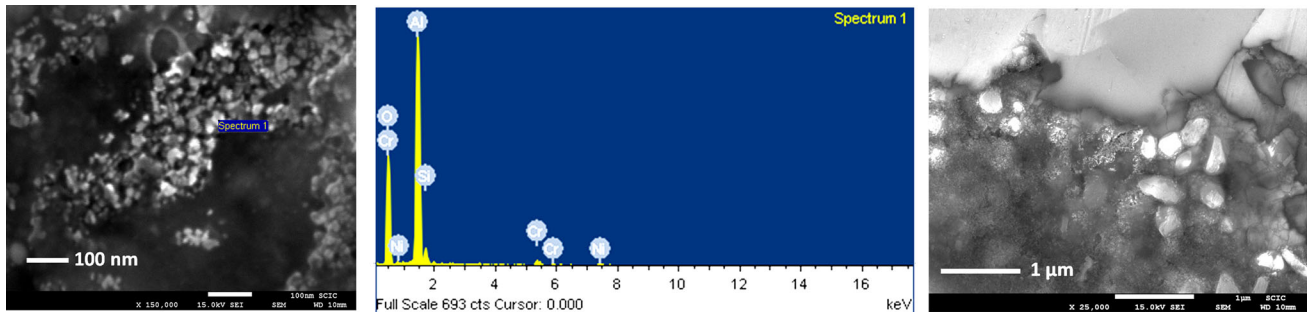

Fig. 8 FEG-SEM micrographs of nanometric alumina particles embedded in the Ni-Cr matrix of NiCrBSi coating
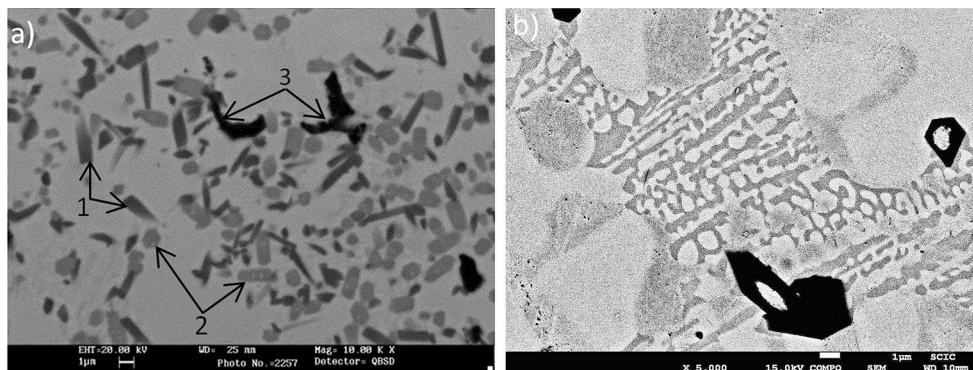

Fig. 9 MEB cross section (lower zone) of NiCrBSi + 12% nanometric alumina showing: (a) diverse phases existing and (b) eutectic morphology

nucleation of a grain around each or a large percentage of nanosized particles with higher surface area, a very fine grain could be obtained.

There are two considerations that are involved in restricting growth by particle pushing: (1) The lower thermal conductivity of the particle affects the temperature gradient ahead of the solidification front and therefore acts as a barrier to the removal of heat necessary for further solidification and (2) the solid particle acts as a barrier preventing solute diffusion away from tip of the growing dendrite, thereby changing the concentration gradient and restricting growth (Ref 44).

XRD and SEM results strongly suggest that the blocky dark gray phase (1) is CrB- and Cr_3B-type chromium boride, and its formation may possibly take place by primary solidification. On the other hand, the light gray phase (2) could be determined as a complex chromium-iron carbide and its formation could occur by a local change of the primary solidification mode. The

formation of carbides and borides during the remelting process of this group of Colmonoy alloys has been previously reported by several authors (Ref 45-47). Moreover, it has been found that, during the solidification of the clad molten pool, it is inevitable that large amounts of eutectics are formed, such as the lamellar eutectic shown in Fig. 9(b).

3.2 Coatings Microhardness

Figure 10 shows the measured microhardness for the three obtained coatings, corresponding to the different powder types tested. The unmodified NiCrBSi alloy presents a uniform hardness value closer to 450 HV with relatively uniform behavior. NiCrBSi + 12% micrometric Al_2O_3 increases hardness around 20.45% but with strong variations, which can be attributed to the micrometric Al_2O_3 particles being dispersed into a weak Ni-based matrix and the heterogeneous distribution

of coarse Cr carbides, while the NiCrBSi + 12% nanometric Al_2O_3 further increases hardness around 50% and has more uniform behavior, with mean value proportional to the Al_2O_3 surface area and higher relative proportions of fine metallic carbides and borides precipitation.

3.3 Abrasive Wear Results

Figure 11 illustrates the roughly linear evolution of volume loss over sliding distance for test applying the same velocity (8.8 m/min).

Abrasive wear behavior of unmodified and modified coatings with micro- and nanometric alumina as a function of normal load applied is shown in Fig. 12. In general, it can be seen that there is significant difference in wear according to changes in normal load, except at lowest load (5 N), where there was a marked reduction in wear rate.

Wear rate versus normal load relationship for unmodified NiCrBSi shows that wear rate is largely governed by the applied load. Increase in wear rate of coating due to increase in normal load depends on the hard microstructure components distribution on the Ni soft matrix.

Influence of alumina addition on wear rate of NiCrBSi coatings. It can be observed that addition of 12% of micrometric alumina lowers the wear rate of coating about 25% under the same sliding conditions. However, nanometric alumina addition lowers the wear rate about 54%. The less cutting extent and lower SiC penetration was found due to the higher hardness and more refined grain structure, and carbide phases distribution along the track is also responsible for different wear rates.

SEM images of wear surface of unmodified coating show the damage increase on wear surface in the form of higher number of microgrooves, and plastic flow of coating in perpendicular direction to sliding direction takes place, Fig. 13(a). Microgrooves are running in sliding direction. Plastic deformation can be seen as extruded fins at the edge of the grooves-produced rubbing. These fins can get detached to form secondary chips when coalescence of cracks takes place. Furthermore, the observation of the worn surface shows that the grooves are step-side and correspond well in size to the abrasive particles used.

The addition of micrometric alumina coating is shown in Fig. 13(b), and it can be observed that the wear surface is not

subjected to as much damage and lower plastic flow as in case of unmodified coating under identical sliding conditions.

NiCrBSi coating with nanometric alumina addition, shows that the damage of the wear surface was found to be a quite
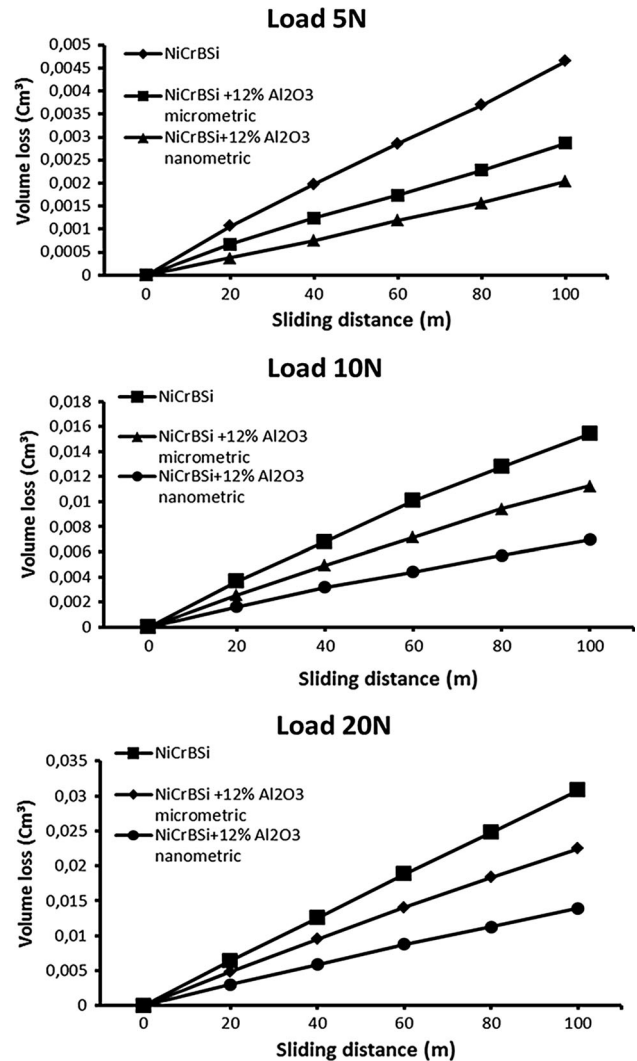

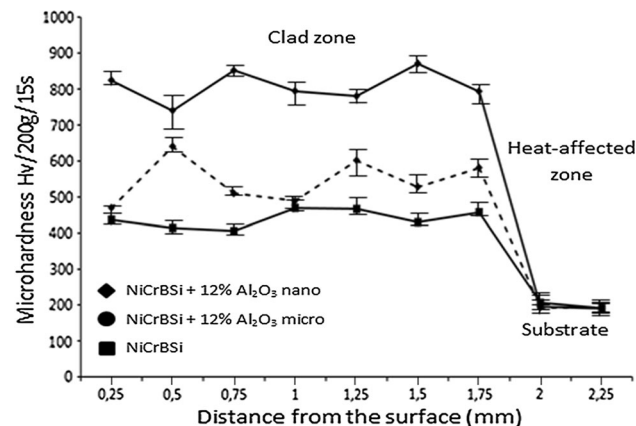Fig. 11 Evolution of volume loss with sliding distance

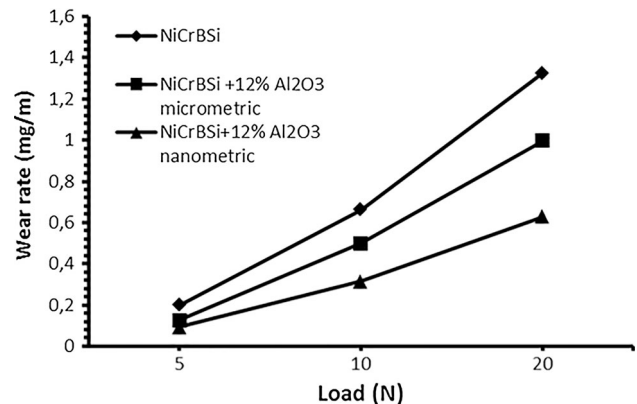Fig. 10 Variation of microhardness in coating/substrate cross section for various coatings

Fig. 12 Wear rate vs. normal load for unmodified NiCrBSi, NiCrBSi + 12% micrometric Al_2O_3 and NiCrBSi + nanometric Al_2O_3

smooth than that with micrometric alumina and the coating presented comparatively lower plastic flow and hence better abrasive wear resistance as show in Fig. 13(c).

### 3.4 Effect of Micro- and Nano-Al_2O_3 on Abrasive Wear Resistance

In this study, it has been found that the microstructure of unmodified NiCrBSi coating is based on solid solution of weak Ni matrix and on other compounds based on CrC and CrB deposited along the grain boundary. The abrasive wear tests of this alloy have demonstrated a higher wear rate which can be attributed to deeper, winder scratches and thereby damage on the soft Ni-Cr matrix, Fig. 14(a). Addition of hard particles of micrometric alumina (lower particles surface area) to comparatively soft Ni-Cr matrix increases the microhardness which, in turn, lowers the damage on wear surface by abrasion. This might

be due to improving the temperature distribution and increasing the cooling rates during the solidification process which enhances the formation of relatively low intensity hard carbide and boride of Cr precipitates on the Ni-Cr matrix. However, wear surface of NiCrBSi + 12% micrometric alumina coating showed craters due to dislodging of Al_2O_3 particles, Fig. 14(b), and brittle fracture of the particles not extracted from the matrix, Fig. 14(c).

Addition of 12% nanometric alumina (higher-particles surface area) produces microstructural change in NiCrBSi coating. This change in morphology has played a major role in improving of abrasive wear behavior, which can be attributed to the: (a) higher surface area of nanometric alumina compared to the micrometric one, (b) higher cooling rate during solidification process and c) formation of high-intensity and well-distributed cuboids of Cr carbide on the Ni-Cr matrix. Also it is expected that alumina addition and the primary crystals of Cr carbide precipitation formed with sharp edges are the possible
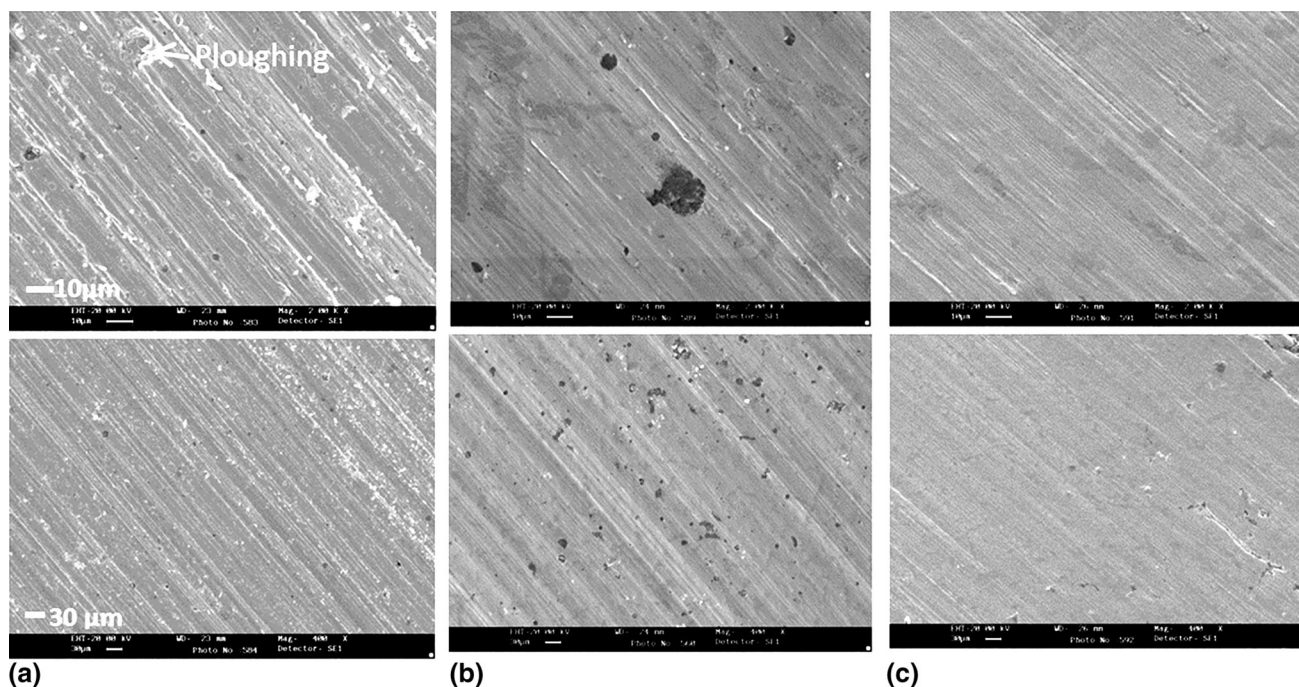
Fig. 13 SEM micrograph of the wear track of: (a) NiCrBSi, (b) 12% micrometric Al_2O_3 dispersion-strengthened NiCrBSi coating, (c) 12% nanometric Al_2O_3 dispersion-strengthened NiCrBSi coating
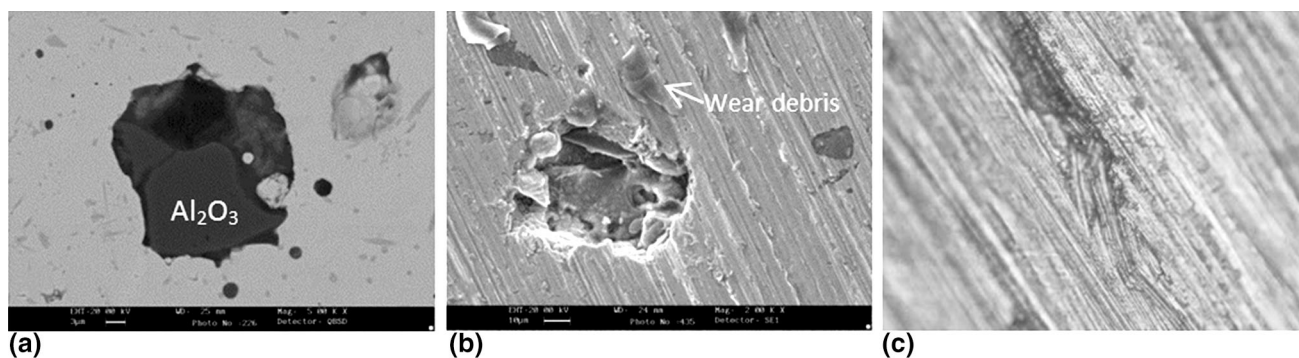
Fig. 14 (a) SEM image of the worn surface of NiCrBSi + 12% micrometric alumina shows a brittle fracture of the micrometric alumina, (b) and (c) damage caused by micrometric alumina reinforcement extracted from the matrix (40 ×)

causes of stress concentrated which increase the Ni matrix hardness.

4. Conclusions

Experimental investigations conducted in the present work to study the effect of Al_2O_3 particles size on abrasive wear of NiCrBSi metal matrix composites have provided the following conclusions:

- Under employed spray conditions, unmodified NiCrBSi, NiCrBSi + 12 wt.% micrometric Al_2O_3 and NiCrBSi + 12 wt.% nanometric Al_2O_3 (both mixed powder) have been deposited by thermal spray technique combined with surface flame melting process to develop coatings of average 1.5 mm thick on AISI 304 stainless steel substrate. Microhardness of the deposited coatings is found to be 450_{200} for unmodified NiCrBSi, 542_{200} for NiCrBSi + 12 wt.% micrometric Al_2O_3 and 813_{200} for NiCrBSi + 12 wt.% nanometric Al_2O_3.
- The microstructure of unmodified NiCrBSi coating layer is mainly composed of Ni-Cr solid solution matrix and hard compounds based on carbide, boride and silicide (CrC, Ni_3B, $NiSi$ and $Ni_{31}Si1_2$) along the grain boundaries.
- The addition of 12 wt.% Al_2O_3 in the NiCrBSi coatings contributes to improving the hard phases (CrC, Ni_3B, $NiSi$ and $Ni_{31}Si_{12}$) distribution on the soft Ni-Cr matrix by increasing the cooling rates after remelting process which in turn depends on the surface area of the Al_2O_3 reinforcement particles.
- The addition of 12 wt.% nanometric Al_2O_3 in the NiCrBSi coatings reduces the grain size of hard phases (CrC, $Ni3B$, $NiSi$ and $Ni_{31}Si_{12}$) from 6-7 μm, obtained with addition of 12 wt.% of micrometric Al_2O_3, to 1-2 μm, which results in a harder coating.
- The abrasive wear rate of the unmodified NiCrBSi coating is 23% higher than the NiCrBSi + 12 wt.% micrometric Al_2O_3, and 86% than the NiCrBSi + 12 wt.% nanometric Al_2O_3. The lower wear rate of NiCrBSi + 12 wt.% nanometric Al_2O_3 is due to higher hardness, more refined and uniformly distributed hard phases (CrC, Ni_3B, $NiSi$ and $Ni_{31}Si_{12}$) on the soft Ni-Cr matrix.

References

1. M. Qian, L.C. Lim, and Z.D. Chen, Laser Cladding of Nickel-Based Hardfacing Alloys, *Surf. Coat. Technol.*, 1998, **106**, p 174–182
2. A. Conde, F. Zubiri, and J. Damborenea, Cladding of Ni-Cr-B-Si Coatings with a High Power Diode Laser, *Mater. Sci. Eng., A*, 2002, **334**(1–2), p 233–238
3. J. Rodríguez, A. Martín, R. Fernández, and J.E. Fernández, An Experimental Study of the Wear Performance of NiCrBSi Thermal Spray Coatings, *Wear*, 2003, **255**, p 950–955
4. P. Wu, X.L. Chen, and E.Y. Jiang, Influence of WC Particle Behavior on the Wear Resistance Properties of Ni-WC Composite Coatings, *Wear*, 2004, **257**(1–2), p 142–147
5. A. Martín, J. Rodríguez, J.E. Fernández, and R. Vijande, Sliding Wear Behaviour of Plasma Sprayed WC-NiCrBSi Coatings at Different Temperatures, *Wear*, 2001, **251**(1–12), p 1017–1022
6. L. Shan-Ping and K. Oh-Yang, Microstructure and Bonding Strength of WC Reinforced Ni-base Alloy Brazed Composite Coating, *Surf. Coat. Technol.*, 2002, **153**(1), p 40–48
7. J.M. Miguel, J.M. Guilemany, and S. Vizcaino, Tribological Study of NiCrBSi Coating Obtained by Different Processes, *Tribol. Int.*, 2003, **36**, p 181–187
8. H.-J. Kim, S.-Y. Hwang, C.-H. Lee, and P. Juvanon, Assessment of Wear Performance of Flame Sprayed and Fused Ni-Based coatings, *Surf. Coat. Technol.*, 2003, **172**(1–2), p 262–269
9. Y. Qiao, T.E. Fischer, and A. Dent, The Effects of Fuel Chemistry and Feedstock Powder Structure on the Mechanical and Tribological Properties of HVOF Thermal-Sprayed WC-Co Coatings with Very Fine Structures, *Surf. Coat. Technol.*, 2003, **172**(1), p 24–41
10. C. Navas, R. Colao, J. De Damborenea, and R. Vilar, Abrasive Wear Behavior of Laser Clad and Flame Sprayed-Melted NiCrBSi Coatings, *Surf. Coat. Technol.*, 2006, **200**, p 6854–6862
11. H. Kim, S. Hwang, C. Lee, and P. Juvanon, Assessment of Wear Performance of Flame Sprayed and Fused Ni-based Coatings, *Surf. Coat. Technol.*, 2003, **172**, p 262–269
12. R. Gonzalez, M. Cadenas, R. Fernández, J.L. Cortizo, and E. Rodríguez, Wear Behaviour of Flame Sprayed NiCrBSi Coating Remelted by Flame or by Laser, *Wear*, 2007, **262**, p 301–307
13. J. Rodríguez, A. Martín, R. Fernández, and J.E. Fernández, An Experimental Study of the Wear Performance of NiCrBSi Thermal Spray Coatings, *Wear*, 2003, **255**, p 950–955
14. J. Kim, S.-Y. Hwang, C.-H. Lee, and P. Juvanson, Assessment of Wear Performance of Flame Sprayed and Fused Ni-Based Coatings, *Surf. Coat. Technol.*, 2003, **172**, p 262–269
15. C. Katsich and E. Badisch, Effect of Carbide Degradation in a Ni-Based Hardfacing Under Abrasive and Combined Impact/Abrasive Conditions, *Surf. Coat. Technol.*, 2011, **206**, p 1062–1068
16. P. Niranatlumpong and H. Korprasert, Phase Transformation of NiCrBSi-WC and NiBSi-WC Arc Sprayed Coatings, *Surf. Coat. Technol.*, 2011, **206**, p 440–445
17. M.R. Ramesh, S. Prakash, S.K. Nath, P.K. Sapra, and B. Venkataraman, Solid Particle Erosion of HVOF-Sprayed WC-Co/NiCrFeSiB Coatings, *Wear*, 2010, **269**, p 197–205
18. P. Kulu and J. Halling, Recycled Hard Metal-Base Wear-Resistant Composite Coatings, *J. Thermal Spray Technol.*, 1998, **7**, p 173–178
19. P. Kulu and T. Pihl, Selection Criteria for Wear Resistant Powder Coatings Under Extreme Erosive Wear Conditions, *J. Thermal Spray Technol.*, 2002, **11**, p 517–522
20. P. Kulu and S. Zimakov, Wear Resistance of Thermal Sprayed Coatings on the Base of Recycled Hardmetal, *Surf. Coat. Technol.*, 2000, **130**, p 46–51
21. A. Zikin, I. Antonov, I. Hussainova, L. Katona, and A. Gavrilović, High Temperature Wear of Cermet Particles Reinforced NiCrBSi Hardfacings, *Trib. Int.*, 2013, **68**, p 45–55
22. H. Sarjas, D. Goljandin, P. Kulu, V. Mikli, A. Surženkov, and P. Vuoristo, Wear Resistant Thermal Sprayed Composite Coatings Based on Iron Self-fluxing Alloy and Recycled Cermet Powders, *Mater. Sci. (Medžiagotyra)*, 2012, **18**, p 34–39
23. K.W.D. Hart, D.H. Harper, M.J. Gill Case studies in wear resistance using HVOF, PTAW and Spray Fusion Surfacing. *1st International Thermal Spray Conference*, Materials Park, OH. ASM International, Montreal, Canada (2000), p 1117–1125
24. A. Klimpel, A. Lisiecki, A. St. Klimpel, and A. Rzeznikiewicz, Robotized GMA Surfacing of Cermetal Deposits, *J. Achiev. Mater. Manuf. Eng.*, 2006, **18**(1–2), p 395–398
25. S. Babu, S. David, R. Martukanitz, and K. Parks, Toward Prediction of Microstructural Evolution During Laser Surface Alloying, *Metall. Mater. Trans. A*, 2002, **33**, p 1189–1200
26. S. Matthews, M. Hyland, and B. James, Microhardness Variation in Relation to Carbide Development in Heat Treated Cr_3C_2-NiCr Thermal Spray Coatings, *Acta Mater.*, 2003, **51**, p 4267–4277
27. J. KJluuttiia, S. Ahmanierni, E. Leivo, P. Sorsa, P. Vuoristo, and T. Mantylat, Wet Abrasion and Slurry Erosion Resistance of Sealed Oxide Coatings, *Proceedings of the 15th International Thermal Spray Conference*, 25-29 May 1998 (1), Nice, France, p 145–150
28. A. Giroud, C. Jouanny, J.L. Heuze, F. Gaillard, and P. Guiraldenq, Friction and corrosion behavior of different ceramic coatings (oxides) obtained by thermal spray for qualification tests in sea water, *Proceedings of the 15th International Thermal Spray Conference*, 25-29 May 1998 (1), Nice, France, p 211–216

29. C. Ding, 1. Li, L Zhang, X. Yu, Wear evaluation of plasma; sprayed oxide and carbide coatings, *Proceedings of the 15th International Thermal Spray Conference*, 25-29 May 1998 (1), Nice. France, p 275–279

30. C. Li, Y. Want, A. Ohmori, and C.C. Berndt, Ed., *Thermal Spray: Surface Engineering Via Applied Research*, ASM International, OH, 2000, p 791

31. T. Ram Prabhu, Investigations of the Effect of Particle Properties on the Wear Resistance of the Particle Reinforce Composites Using a Novel Wear Model, *Int. J. Comput. Mater. Sci. Eng.,* 2016, **5**(02). doi: 10.1142/S2047684116500135

32. S. Natarajan, E. Anand, K.S. Akhilesh, and A. Rajagopal, Effect of Addition on the Microstructure, Hardness and Abrasive Wear Behavior of Plasma Sprayed NiCrBSi Coatings, *Mater. Chem. Phys.*, 2016, **175**, p 100–106

33. S. Harsha, D.K. Dwivedi, and A. Agrawal, Influence of WC Addition in Co-Cr-W-Ni-C Flame Sprayed Coatings on Microstructure Microhardness and Wear Behaviour, *Surf. Coat. Technol.*, 2007, **201**, p 5766–5775

34. S.J. Gregg, and K.S.W. Sing, *Adsorption, Surface Area and Porosity. 2. Auflage,* Academic Press, London 1982, 303 Seiten

35. S. Lowell, and J.E. Shields, *Powder Surface Area and Porosity, Technology & Engineering,* 1991, p 252

36. F. Rouquerol, J. Rouquerol, and K. Sing, *Adsorption by Powder and Porous Solids: Principles, Methodology and Applications,* Elsevier, 1999, ISBN: 978012598920

37. S. Brunauer, P.H. Emmett, and E. Teller, Adsorption of Gases in Multimolecular Layers, *J. Am. Chem. Soc.*, 1938, **60**, p 309–319

38. T. Gómez-del Río, M.A. Garrido, J.E. Fernández, M. Cadenas, and J. Rodríguez, Influence of the Deposition Techniques on the Mechanical Properties and Microstructure of NiCrBSi Coatings, *J. Mater. Process. Technol.*, 2008, **204**(1–3), p 304–312

39. D. Guo, F. Li, J. Wang, and J. Sun, Effects of Post-coating Processing on Structure and Erosive Wear Characteristics of Flame and Plasma Spray Coatings, *Surf. Coat. Technol.*, 1995, **73**(1–2), p 73–76, 78

40. R. Zieris, S. Nowotny, L. Berger, L. Haubold, and E. Beyer, *International Thermal Spray Conference: Advancing the Science and Applying the Technology*, ASM International, OH, 2003, p 567–577

41. R. Vilar, Laser Cladding, *Laser Appl.*, 1999, **11**, p 64

42. K.I. Dragnevski, A.M. Mullis, and R.F. Cochrane, The Effect of Experimental Variables on the Levels of Melt Undercooling, *Mater. Sci. Eng.*, 2004, **A375–377**, p 485–487

43. A. French and W. Kurz, Microstructural Effects on the Sliding Wear Resistance of a Cobalt-Based Alloy, *Wear*, 1994, **174**(1–2), p 81–91

44. J.K. Kim and R.K. Rohatgi, An Analytical Solution of the Critical Interface Velocity for the Encapturing of Insoluble Particles by a Moving Solid/Liquid Interface, *Met. Trans. A*, 1998, **29**, p 351–358

45. D.W. Zhang, T. Lei, and Ch Chen, The Effects of Heat Treatment on Microstructure and Erosion Properties of Laser Surface-Clad Ni-Base Alloy, *Surf. Coat. Technol.*, 1999, **115**, p 176–183

46. Z. Dawei, T. Li, and T.C. Lei, Laser Cladding of Ni-Cr$_3$C$_2$/(Ni + Cr) Composite Coating, *Surf. Coat. Technol.*, 1998, **110**, p 81–85

47. R.I. Terzona, D.N. Allopp, and I.M. Hutchings, Transitions Between Two-Body and Three-Body Abrasive Wear: Influence of Test Conditions in the Microscale Abrasive Wear Test, *Wear*, 1999, **225–229**, p 205–214